



Cite this: DOI: 10.1039/d0nj02056g

Asymmetric zinc porphyrin derivatives bearing three pseudo-pyrimidine *meso*-position substituents and their photosensitization for H₂ evolution†

 Peng Zeng,^{‡,ab} Ya Zheng,^{‡,b} Shengtao Chen,^b Haoran Liu,^b Renjie Li^{id}*^b and Tianyou Peng^{id}*^b

Novel asymmetric zinc porphyrin derivatives (ZnPy-5 and ZnPy-6) with *meso*-positions bearing one benzoic acid and three pseudo-pyrimidines with two N atoms located at different positions were synthesized and utilized as sensitizers for Pt-loaded g-C₃N₄ (PCN). Compared to the analogue (ZnPy-1 bearing one benzoic acid and three phenyl *meso*-position substituents), ZnPy-5 and ZnPy-6 exhibit significantly enhanced photosensitization on PCN under visible light ($\lambda \geq 420$ nm) illumination. In particular, ZnPy-5/PCN and ZnPy-6/PCN exhibit H₂ evolution activities of 418 and 585 $\mu\text{mol h}^{-1}$, corresponding to turnover numbers (TON) of 8845 and 12 381 h^{-1} , respectively. Both of these values are much better than (316 $\mu\text{mol h}^{-1}$) of ZnPy-1/PCN, which has a TON of 6687 h^{-1} . In addition, ZnPy-5/PCN and ZnPy-6/PCN show apparent quantum yields of 32.6% and 33.1% at 420 nm monochromatic light, and these are much higher than that (10.6%) for ZnPy-1/PCN. Compared with ZnPy-5, the two N atoms of the pseudo-pyrimidines in ZnPy-6 are further away from the porphyrin macrocycle, which can more effectively combine with the sacrificial reagent and g-C₃N₄, thus promoting dye regeneration and the photoexcited charge transfer for delivering better photocatalytic performance. The present results demonstrate that the number and positions of the N atoms in the peripheral substituents of the porphyrin derivatives have a great influence on the photosensitization, and that the fine-tuning of molecular structures is crucial for improving the H₂ evolution activity of the dye-sensitized semiconductors.

 Received 23rd April 2020,
 Accepted 29th May 2020

DOI: 10.1039/d0nj02056g

rsc.li/njc

Introduction

As an ideal energy carrier, hydrogen (H₂) will be the main energy source in the foreseeable future since it can be produced through water-splitting using a variety of energy sources such as fossils, nuclear energy and solar energy. Among the various hydrogen production techniques, photocatalytic H₂ evolution from water-splitting using sunlight has attracted considerable attention due to it being cost-effective and eco-friendly.^{1–5} Up to now, inorganic semiconductors such as metal oxides, metal sulfides and metal nitrides have been the most extensively used photocatalysts.^{6–12} Among them, the most widely investigated

TiO₂ with a wide bandgap can only absorb UV photons that account for merely 4–5% of sunlight.^{1,6} Therefore, great efforts have been made to explore new photocatalysts, enabling the efficient utilization of visible light since it represents ~50% of sunlight (AM1.5).^{1,6}

Among the many strategies used to harvest visible light, photosensitization is an effective way to extend the spectral response range of the semiconductors with a wide bandgap.^{6,13–19} As a light-harvesting center, the sensitizer must have a series of basic requirements, including a broad spectral response range, an appropriate redox potential for efficient electron injection and dye regeneration, long-term irradiation stability and low cost.^{6,13–17} Currently, a number of organic compounds and metal complexes such as Eosin Y (EY),¹³ poly(3-hexylthio-phenylene) (P3HT),¹⁴ and metal phthalocyanines (MPC)^{15,16} have been used as a sensitizer for semiconductors with a wide bandgap to achieve a visible-light-responsive ability for H₂ evolution. Metal porphyrin and its derivatives have also attracted great interest as sensitizers in mimicking the natural photosynthesis due to their strong photo-absorption ability in the visible region (with a strong

^a School of Food and Pharmaceutical Engineering, Zhaoqing University, Zhaoqing 526061, P. R. China

^b College of Chemistry and Molecular Sciences, Wuhan University, Wuhan 430072, P. R. China. E-mail: lirj@whu.edu.cn, typeng@whu.edu.cn

 † Electronic supplementary information (ESI) available: MALDI-TOF and ¹H MNR spectra, cyclic voltammograms, photoluminescence and UV-vis absorption spectra. See DOI: 10.1039/d0nj02056g

‡ These authors contributed to this work equally.

B-band around ~ 420 nm and moderate Q-bands in the range of 500–650 nm) and thermal stability.^{17,18} For example, an iron porphyrin derivative ((FeTPP)₂O) was found to be an efficient sensitizer of *g*-C₃N₄ for H₂ evolution due to its π - π interactions and Fe–N bonding.¹⁸

Recently, asymmetric zinc porphyrins (ZnPy) bearing one benzoic acid and three pseudo-pyridine peripheral substituents were utilized by our group to sensitize Pt-loaded *g*-C₃N₄ for visible-light-driven H₂ evolution.^{20–22} It was found that the different steric positions of the N atom in the pseudo-pyridines resulted in different interactions between the porphyrin and ascorbic acid (AA) as the sacrificial reagent, and this strongly influenced the photocatalytic activity. Among them, the ZnPy derivative with the lowest steric hindrance of the N atom in the pseudo-pyridines delivered the best photosensitization. When the three pseudo-pyridines were substituted with phenyls, however, the corresponding ZnPy derivative showed significantly decreased photosensitization.^{20,21} One possible reason for this is that the two lone-pair electrons and basicity of the N atom of the pyridine increase the electron cloud density of the ZnPy molecules and therefore its interaction with AA and *g*-C₃N₄. This can promote the charge transfer and dye regeneration, and then promote the photoactivity of the dye-sensitized system. Similarly, a pyrimidine with two N atoms that was introduced into a dye (INPA) linked to a carboxylic acid facilitated the interaction between the dye and TiO₂, and therefore enhanced the photovoltaic performance of the dye-sensitized solar cells (DSSCs).²³ Density functional theory (DFT) calculations also demonstrated that when a pyrimidine group is introduced in a p-type sensitizer of DSSCs, it can result in an increased charge transfer ability compared to with the introduction of a thiophene group.²⁴ These results imply that pyrimidines (with two N atoms) as peripheral groups, when introduced in ZnPy derivatives, might more effectively increase the electron density of the porphyrin macrocycle and its interaction with AA, and thus would be a benefit to dye regeneration and photo-sensitization on semiconductors.

Herein, novel asymmetric zinc porphyrin derivatives (ZnPy-5 and ZnPy-6) with *meso*-positions bearing one benzoic acid and three pseudo-pyrimidines (Scheme 1) were designed and synthesized, and they were then utilized as sensitizers for Pt-loaded *g*-C₃N₄ (hereafter denoted as PCN) for visible-light-driven H₂ evolution. In Scheme 1, ZnPy-1, with one benzoic acid and three phenyl *meso*-position substituents, is the contrast



Scheme 1 Molecular structures of the ZnPy derivatives.

sample, while ZnPy-5 and ZnPy-6 contain one benzoic acid and three pseudo-pyrimidines, the two N atoms of which are located at different positions, and the two N atoms of the pseudo-pyrimidines in ZnPy-6 are further away from the porphyrin macrocycle compared with those in ZnPy-5. The experimental results show that both ZnPy-5 and ZnPy-6 deliver much better photosensitization on PCN than ZnPy-1 under visible light ($\lambda \geq 420$ nm) illumination, and that ZnPy-6/PCN delivers higher H₂ evolution activity than ZnPy-5/PCN. The above differences in the photosensitization of these ZnPy derivatives on PCN and the effect of the number and positions of the N atoms in the peripheral substituents of the porphyrin on the photo-activity were studied in detail, in order to investigate more efficient porphyrin-based sensitizers and their regeneration processes in artificial photosynthesis.

Results and discussion

Spectroscopic analyses

The obtained ZnPy derivatives (ZnPy-5 and ZnPy-6) were identified using spectroscopic characterization techniques (¹H nuclear magnetic resonance (NMR) spectroscopy; matrix assisted laser desorption/ionization time-of-flight mass spectrometry (MALDI-TOF-MS); ultraviolet visible (UV-vis), Fourier-transform infrared (FTIR) and fluorescence spectroscopies) and elemental analysis (see Fig. S1–S8 and the Experimental section, ESI[†]). UV-Vis absorption spectra (Fig. 1a) show that the metal-free porphyrin derivative (H₂Py-5) in DMF solution has five obvious absorption bands with maximum absorption wavelengths (λ_{\max}) at ~ 416 nm (B-band), 511 nm (Q-band), 546 nm (Q-band), 587 nm (Q-band) and 642 nm (Q-band). H₂Py-6 displays a similar absorption spectrum but with a bathochromic shift of ~ 2 nm relative to the corresponding absorption bands of H₂Py-5.

After coordination with Zn²⁺, the resulting ZnPy-5 and ZnPy-6 exhibit very similar absorption spectra (Fig. 1b) with one strong B-band in the range of 350–450 nm, due to the $a_{1u}(\pi)$ to $e_g^*(\pi)$ electronic transitions and two less intensive Q-bands in the range of 450–670 nm that arise from the $a_{2u}(\pi)$ to $e_g^*(\pi)$ electronic transitions.^{20–22} In particular, ZnPy-5 and ZnPy-6 show respective B-bands at a λ_{\max} of ~ 425 and ~ 427 nm (Fig. 1b), with both of them redshifted by ~ 9 nm compared with those of H₂Py-5 and H₂Py-6 (Fig. 1a), respectively.

Similar to the metal-free porphyrins (H₂Py-5 and H₂Py-6), the absorption spectrum of ZnPy-6 also shows a bathochromic shift of ~ 2 nm with respect to that of ZnPy-5, and this can be ascribed to the different positions of the two N atoms in the pseudo-pyrimidine substituents (Scheme 1). Compared with ZnPy-5 (or H₂Py-5), ZnPy-6 (or H₂Py-6) has the two N atoms in the peripheral pseudo-pyrimidines further away from the porphyrin macrocycle, and this could weaken the electron-withdrawing ability of the pseudo-pyrimidines and increase the electron cloud density of the porphyrin macrocycle, thus enhancing the photo-absorption ability, as shown in Fig. 1.

The FTIR spectra (Fig. 2) indicate that the porphyrin macrocycles have their characteristic IR absorption bands in the range

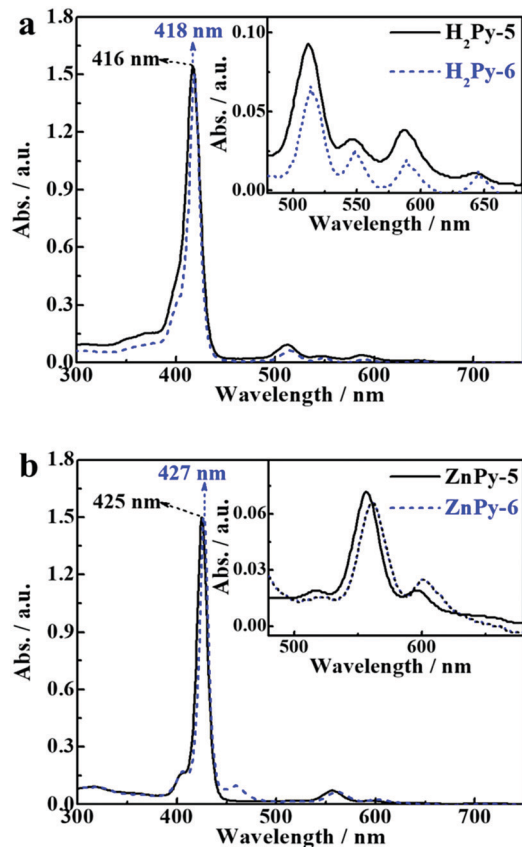


Fig. 1 UV-vis absorption spectra of (a) the metal-free porphyrins (H_2Py-5 and H_2Py-6) and (b) the zinc porphyrins ($ZnPy-5$ and $ZnPy-6$) in DMF solution.

of $700\text{--}799\text{ cm}^{-1}$, originating from the out-of-plane bending vibration of $=C-H$ in the pyrrole rings, and the characteristic IR peak at 793 cm^{-1} can be assigned to the *p*-disubstituted benzene of the porphyrin derivatives. In addition, the broad IR peak near 3426 cm^{-1} can be attributed to the stretching vibration of $O-H$ in the $-COOH$ group and the H-bond between the $-COOH$ groups.²⁰ The metal-free porphyrin derivatives (H_2Py-5 and H_2Py-6) exhibit IR peaks at 952 and 965 cm^{-1} , which can be ascribed to the $N-H$ vibration in the pyrrole rings (Fig. 2a), but the peaks disappear after the coordination with Zn^{2+} for $ZnPy-5$ and $ZnPy-6$. In addition, $ZnPy-5$ and $ZnPy-6$ display their featured stretching vibration band of $N-Zn$ at 995 cm^{-1} . In particular, the pseudo-pyrimidines in the porphyrin derivatives create the IR peaks that are mainly located at ~ 1566 and $\sim 1408\text{ cm}^{-1}$, and these positions are slightly different due to the different positions of the two N atoms in the pseudo-pyrimidines of the $ZnPy$ derivatives.

UV-vis diffuse reflectance absorption spectra (DRS) of the $ZnPy$ derivative ($ZnPy-5$ and $ZnPy-6$) sensitized Pt-loaded $g-C_3N_4$ (PCN) complexes are depicted in Fig. 3. As seen in the spectra, the pristine PCN exhibits an absorption edge at $\sim 450\text{ nm}$ in addition to an absorption tail that is probably due to the $n-\pi^*$ electronic transitions.²⁰⁻²² $ZnPy-5/PCN$ and $ZnPy-6/PCN$ display the absorption features of the combination of PCN with the $ZnPy$ derivatives, but the adsorption bands in the range of $420\text{--}650\text{ nm}$ are much broader than their respective $ZnPy$

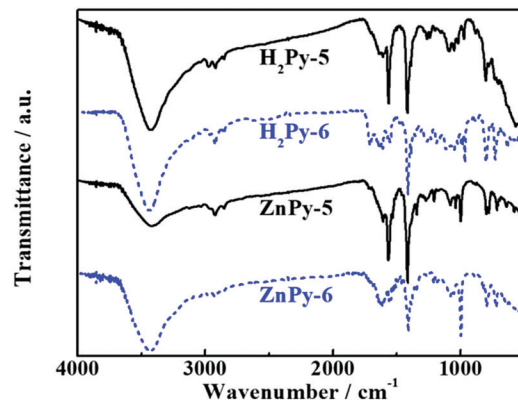


Fig. 2 FTIR spectra of the metal-free porphyrins (H_2Py-5 and H_2Py-6) and zinc porphyrins ($ZnPy-5$ and $ZnPy-6$).

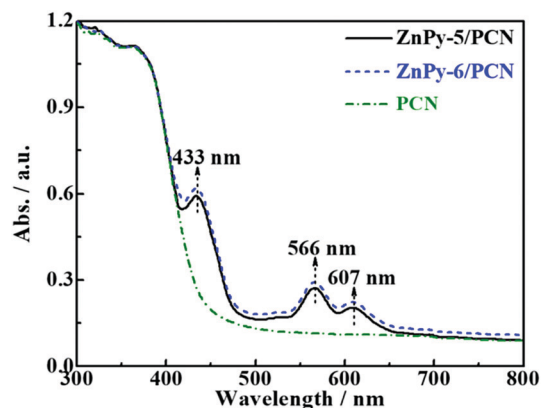


Fig. 3 UV-vis diffuse reflectance absorption spectra (DRS) of PCN and its dye-sensitized products ($ZnPy-5/PCN$ and $ZnPy-6/PCN$).

derivative in DMF solution (Fig. 1a). The slight redshifts ($\sim 8\text{ nm}$) and enhanced peak intensities of those B-band and Q-band absorptions may be caused by the $\pi-\pi$ stacking interaction between the $ZnPy$ molecules and $g-C_3N_4$ in terms of their similar π -conjugated and planar structures.^{15,25-27} Furthermore, the slight redshifts can be due to the chemical interaction between the $-COOH$ of the $ZnPy$ derivatives and the terminal $-NH$ of $g-C_3N_4$ via a condensation reaction.^{9,21} With the same dye-loading content, $ZnPy-6/PCN$ delivers slightly higher peak intensities than $ZnPy-5/PCN$. The possible reason for this is that the two N atoms of the pseudo-pyrimidines in $ZnPy-6$ are further away from the macrocycle, and this results in the electron-withdrawing ability not being as strong as that of $ZnPy-5$, thus the macrocycle of $ZnPy-6$ has more concentrated electron density than the macrocycle of $ZnPy-5$. This then causes $ZnPy-6$ to be more easily adsorbed and aggregated on PCN, enhancing the photo-absorption ability.

Energy band structure analyses and theoretical calculations

Fig. 4 depicts the normalized UV-vis absorption and fluorescence (FL) spectra of $ZnPy-5$ and $ZnPy-6$ at the same concentration in DMF solution. As seen from the spectra, both $ZnPy-5$ and $ZnPy-6$ have a maximum emission wavelength of 610 nm at

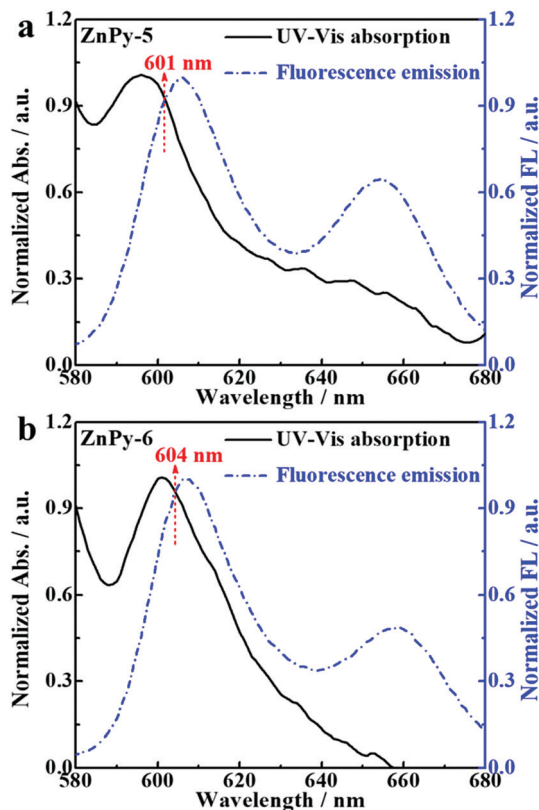


Fig. 4 Normalized UV-vis absorption and fluorescence emission spectra of ZnPy-5 and ZnPy-6 in DMF solution with $\lambda_{\text{ex}} = 426$ nm.

$\lambda_{\text{ex}} = 426$ nm. It has been reported that the optical bandgap (E_{0-0}) of porphyrins can be estimated from the intersection point wavelength (λ_{int}) of the normalized absorption and emission spectra (Fig. 4) using the formula, $E_{0-0} = (1240/\lambda_{\text{int}})$.^{27,28} ZnPy-5 and ZnPy-6 exhibit intersection point wavelengths at 601 and 604 nm, corresponding to E_{0-0} values of 2.06 and 2.05 eV (Table 1), respectively.

From the cyclic voltammograms (CV in Fig. S9, ESI[†]) of the ZnPy derivatives in DMF solution, corresponding electrochemical data can be estimated by a tangent method and the data are summarized in Table 1,²⁹ in which E_{ox} (V vs. NHE) is calculated from the Leeuw formula [E_{ox} (V vs. Ag/AgNO₃) - $E_{1/2}$ (Fc⁺/Fc vs. Ag/Ag⁺) + $E_{1/2}$ (Fc⁺/Fc vs. NHE)].³⁰⁻³² The highest occupied molecular orbital (HOMO) of the ZnPy derivative corresponds to the E_{ox} value,²⁰⁻²³ and the lowest unoccupied molecular orbital (LUMO) can be estimated using the equation, $E^* = E_{\text{ox}} - E_{0-0}$ (Table 1). Based on these results, the corresponding experimental LUMO/HOMO levels of the ZnPy derivatives can be plotted as shown in Fig. 5, in which the energy band structure, including the conduction band (CB) and valence band (VB), of g-C₃N₄ is also depicted. It can be seen that both ZnPy-5 and ZnPy-6 have a LUMO energy level (E^*) of -1.16 V, which is slightly more negative than the CB (-1.12 V) of g-C₃N₄.³³ This indicates that the photogenerated electrons of these excited state ZnPy derivatives can readily be injected into the CB of g-C₃N₄ due to thermodynamics.

Table 1 Spectroscopic and electrochemical data of the obtained ZnPy derivatives

Dye	$\lambda_{\text{max}}/\text{nm}$	$\log \epsilon$	E_{ox}/V (vs. NHE)	E_{0-0}/eV	E^*/V
ZnPy-5	425	5.87	0.90	2.06	-1.16
ZnPy-6	427	5.90	0.89	2.05	-1.16
ZnPy-1 ^b	426	5.77	0.91	2.05	-1.14

^a Calculated with formula, $E^* = E_{\text{ox}} - E_{0-0}$. ^b Data from ref. 20.

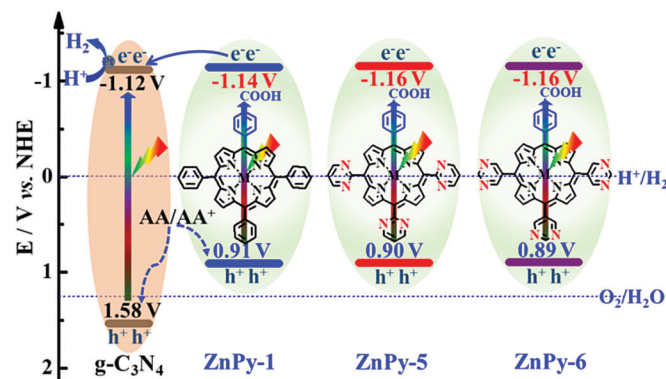


Fig. 5 Experimental values of the molecular orbital energy levels of the ZnPy derivatives and the VB/CB levels of g-C₃N₄.

DFT calculations were carried out on the ZnPy derivatives at the B3LYP/6-31G(d) level to explore their energy level distribution and electron transfer. The calculated frontier orbital energy levels (Fig. 6) indicate that the HOMO-2 electrons of the ZnPy derivatives are mainly concentrated around the metal center, and the HOMO-1 and HOMO electrons are delocalized over the porphyrin macrocycles.³⁴ On the other hand, the LUMO+1 and LUMO electrons of the π^* orbitals are delocalized across the porphyrin macrocycle and move towards the carboxyl group, whereas the LUMO+2 electrons are mainly localized over the benzene ring and the carboxyl group. These frontier molecular orbitals of ZnPy-5 and ZnPy-6 demonstrate that the photoexcited electrons can transfer from the metal center of porphyrin towards the carboxyl group,³⁴ and this would facilitate the directional injection of electrons into chemically bonded g-C₃N₄ for H₂ evolution.^{20,25-27}

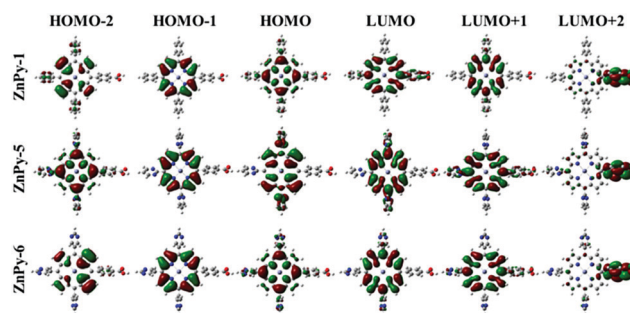


Fig. 6 Frontier molecular orbitals of ZnPy-1, ZnPy-5 and ZnPy-6, fully optimized at the B3LYP/6-31G level.

Photocatalytic performance analyses

The photoreaction conditions can influence the photoactivity of a dye-sensitized semiconductor.^{4,6,35} Considering the similarity between the present dye-sensitized Pt-loaded $g\text{-C}_3\text{N}_4$ and our previous systems,^{20–22} we adopted a similar photoreaction condition, as follows: 15 mg of 1.5 wt% Pt/ $g\text{-C}_3\text{N}_4$ (PCN), sensitized with the ZnPy derivatives dispersed in 10 mL of ascorbic acid (AA) aqueous solution (50 mM). Rotary evaporation was conducted to load the ZnPy derivative in order to ensure the same dye-loading content ($6.30 \mu\text{mol g}^{-1}$), and this was confirmed by a desorption experiment.

Fig. 7a depicts the photocatalytic H_2 evolution activity of the obtained PCN and its dye-sensitized products under visible light ($\lambda \geq 420 \text{ nm}$) illumination. As seen from the figure, the ZnPy derivatives that are loaded onto PCN show clear photosensitization for H_2 evolution compared with the pristine PCN that only delivers a H_2 evolution activity of $112 \mu\text{mol h}^{-1}$. As mentioned above, the asymmetric structures of the ZnPy derivatives can promote the movement of intramolecular directed electrons from the metal center towards the carboxyl group, and the more negative LUMO levels than the CB of $g\text{-C}_3\text{N}_4$ (Fig. 5) are beneficial for the excited state electrons to transfer from porphyrin to $g\text{-C}_3\text{N}_4$ connected *via* the carboxyl groups.^{9,20,21} This conjecture can be corroborated by the photoluminescence (PL)

spectra (Fig. S10a and b, ESI[†]). It can be seen that both ZnPy-5 and ZnPy-6 in DMF solution exhibit a strong emission band at $\lambda_{\text{ex}} = 426 \text{ nm}$, implying fast charge recombination of their excited states. After addition into PCN, the emission intensities of both ZnPy-5 and ZnPy-6 were significantly reduced, indicating that the charge recombination rate of the porphyrin derivatives can clearly be slowed down by the addition of PCN.^{36–38} The time-resolved fluorescence spectra (TRFS) indicate that the fluorescence lifetimes (τ) of the ZnPy-5 and ZnPy-6 solutions can be decreased by adding PCN (Fig. S10c and d, ESI[†]), and this also confirms that a charge transfer process exists from the two ZnPy dyes to the PCN, since $g\text{-C}_3\text{N}_4$ does not absorb 475 nm light.³⁹ This issue is also supported by the transient photocurrent curves of a dye-sensitized PCN suspension irradiated with $\lambda \geq 420 \text{ nm}$ light (Fig. S11, ESI[†]). Compared to pristine PCN, both ZnPy-5/PCN and ZnPy-6/PCN exhibit clearly enhanced photocurrent values, suggesting that the photoexcited charge carriers of the porphyrin derivatives can be efficiently transferred and separated. The above results confirm that the fast charge separation is the main reason for the clear photosensitization for H_2 evolution of the ZnPy derivatives on PCN (Fig. 7a).

Moreover, ZnPy-5 and ZnPy-6 on PCN exhibit a much better photosensitization performance than the contrast sample (ZnPy-1) bearing three peripheral phenyls (Scheme 1). For instance, ZnPy-5/PCN and ZnPy-6/PCN exhibit H_2 evolution activities of 418 and $585 \mu\text{mol h}^{-1}$ (Fig. 7a), corresponding to turnover numbers (TONs) of 8845 and 12381 h^{-1} , respectively. Both of these values are much better than that ($316 \mu\text{mol h}^{-1}$ with a TON of 6687 h^{-1}) of ZnPy-1/PCN. This implies that the pyrimidines that replace the phenyls in ZnPy-1 are responsible for more efficient photosensitization of ZnPy-5 and ZnPy-6, and this is similar to our previous results.^{20–22} Since ascorbic acid (AA) as an acidic sacrificial reagent can provide electrons to regenerate the oxidized dye molecules, the ZnPy derivatives with three basic pyridine substituents can form an electron transfer channel through proton coupling with AA to promote dye regeneration, and thus deliver better H_2 evolution activity than ZnPy-1 bearing three phenyls.^{20,21} It is possible that the two N atoms of the three pseudo-pyrimidines in ZnPy-5 and ZnPy-6 greatly benefit the proton coupling process with AA molecules, and this then contributes to more efficient dye regeneration compared to ZnPy-1 without pseudo-pyrimidines. Therefore, the substitution of pseudo-pyrimidines for phenyls in ZnPy-1 and the effective electron transfer from the dye to $g\text{-C}_3\text{N}_4$ should be the main reasons for the better photoactivity of ZnPy-5/PCN and ZnPy-6/PCN compared with ZnPy-1/PCN (Fig. 7a).

In addition, the H_2 evolution activity ($585 \mu\text{mol h}^{-1}$) of ZnPy-6/PCN is much better than that ($418 \mu\text{mol h}^{-1}$) of ZnPy-5/PCN under the same photoreaction conditions. Since ZnPy-5 and ZnPy-6 have very similar absorption spectra, molar extinction coefficients, photoelectrochemical properties and energy band structures (Table 1 and Fig. 5),²⁰ implying their similar driving force for the photoexcited electrons of the dye injecting into the PCN, the difference in H_2 evolution performance between the two dye-sensitized products can be mainly attributed to the differences in the peripheral substituents. ZnPy-6 has its

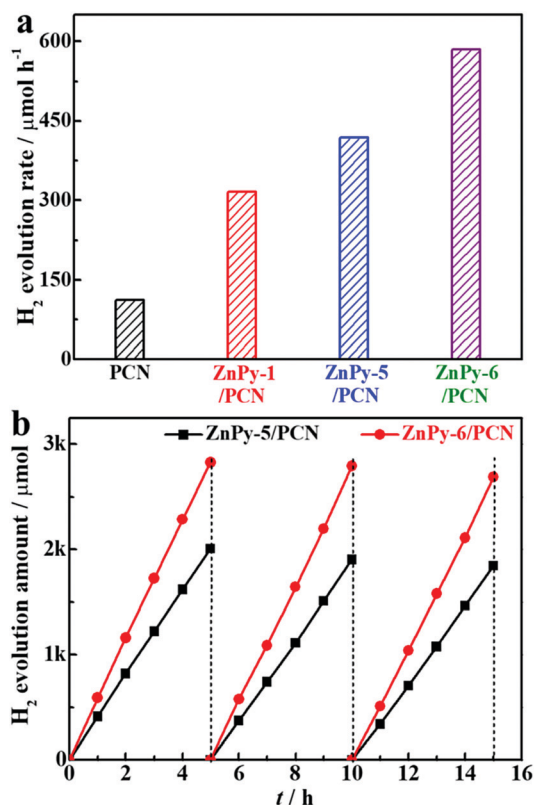


Fig. 7 (a) Comparison of H_2 evolution rates over the PCN and its dye-sensitized products (ZnPy-5/PCN and ZnPy-6/PCN). (b) Time course of H_2 evolution over ZnPy-5/PCN and ZnPy-6/PCN. Conditions: 15 mg photocatalyst, 10 mL of AA solution (50 mM), 1.5 wt% Pt-loading, $6.30 \mu\text{mol g}^{-1}$ dye adsorbed and $\lambda \geq 420 \text{ nm}$ light irradiation.

two N atoms in the pseudo-pyrimidine groups further away from the porphyrin macrocycle than the ZnPy-5 does. This means that ZnPy-6 has a lower steric hindrance than ZnPy-5 when the two N atoms in the pseudo-pyrimidines combine with AA molecules through proton coupling, hence promoting the regeneration of the oxidized dye molecules.⁴⁰ Since *g*-C₃N₄ has rich surface features such as basicity, electron-rich and H-bonds,^{41–44} the N atoms that are further away from the porphyrin macrocycle in ZnPy-6 are more easily combined with *g*-C₃N₄ *via* H-bonds than those in ZnPy-5, hence promoting the photogenerated electron transfer from porphyrin to the semiconductor for the photocatalytic reaction.

The above conjecture can be validated by the changing trends of PL, TRFS spectra and transient photocurrent curves. For example, ZnPy-6 in DMF solution presents more obvious fluorescence quenching than ZnPy-5 after the addition of PCN (Fig. S10a and b, ESI[†]). The fluorescence lifetime (τ) decrease of ZnPy-6 with the addition of PCN is 51% (from 3.09 ns to 1.51 ns), and this is more obvious than the decrease (45% from 3.12 ns to 1.73 ns) of ZnPy-5 when PCN is added (Fig. S10c and d, ESI[†]), and this also indicates that the electron transfer between ZnPy-6 and PCN is faster than that between ZnPy-5 and PCN. In addition, ZnPy-6/PCN shows a more obvious higher photocurrent than ZnPy-5/PCN (Fig. S11, ESI[†]). The above results demonstrate that the electron transfer between ZnPy-6 and PCN is more efficient than that between ZnPy-5 and PCN, and this is consistent with the above-mentioned changing trends of photoactivity (Fig. 7a). Therefore, it can be concluded that ZnPy derivatives, with their N atoms further away from the porphyrin macrocycle, are not only beneficial for dye regeneration, but they also promote charge separation and transfer for efficient H₂ evolution.

According to our previous literature,²⁰ ZnPy-2 and ZnPy-3 with pseudo-pyridines as peripheral substituents have N positions similar to those in ZnPy-5 and ZnPy-6 bearing three pseudo-pyrimidines with two N atoms, respectively. The corresponding ZnPy-2/PCN and ZnPy-3/PCN delivered H₂ evolution activities of 316 and 451 $\mu\text{mol h}^{-1}$,²⁰ respectively. It is apparent that the present ZnPy-5 and ZnPy-6 on PCN have more effective photosensitization than ZnPy-2 and ZnPy-3 under the same photoreaction conditions (Fig. 7a). This indicates that porphyrin-bearing pseudo-pyrimidines with two N atoms exhibit better H₂ evolution activity than the derivatives bearing pseudo-pyridines with one N atom. There are two possible reasons for this issue: (1) the increase in N atoms in the pseudo-pyrimidines of ZnPy-5 and ZnPy-6 can promote a more efficient excited state charge transfer than that of ZnPy-2 and ZnPy-3; (2) the additional N atoms in the pseudo-pyrimidines of ZnPy-5 and ZnPy-6 can more effectively interact with the sacrificial reagent (AA) through proton coupling to promote electron transfer and dye regeneration, compared to ZnPy-2 and ZnPy-3.^{20–22} Namely, the basic pseudo-pyrimidine substituents in ZnPy-5 and ZnPy-6 are beneficial for the proton coupling process with acidic AA molecules, and this then causes more efficient hole consumption and dye regeneration, and thus better photosensitization than the porphyrin derivatives bearing phenyls (*e.g.* ZnPy-1) or

pseudo-pyridines (ZnPy-2 and ZnPy-3).²⁰ Therefore, it can be concluded that increasing the number of N atoms in the peripheral groups can improve the photocatalytic H₂ evolution activity to a certain extent.

Fig. 7b displays the photostability of dye-sensitized PCN for visible-light-responsive H₂ evolution under the above photo-reaction conditions. As seen from the figure, both ZnPy-5/PCN and ZnPy-6/PCN show sustained enhancement in H₂ evolution and fairly good stability for a total of 15 h in the three consecutive runs with fresh sacrificial reagent solution periodically replaced during each run. Under $\lambda \geq 420$ nm light illumination, the average H₂ evolution activity over ZnPy-5/PCN is 402 $\mu\text{mol h}^{-1}$ in the first run of 5 h, and this subsequently declines to 381 and 369 $\mu\text{mol h}^{-1}$ in the second and third runs, whilst the activity retention for the third run is $\sim 92\%$ compared to the first run. Similarly, the average H₂ evolution activity over ZnPy-6/PCN is 565 $\mu\text{mol h}^{-1}$ in the first run, and this decreases to 558 and 537 $\mu\text{mol h}^{-1}$ in the second and third runs, whilst the activity retention ratio for the third run is $\sim 95\%$ compared to the first run. These results demonstrate that both ZnPy-5 and ZnPy-6 on PCN have excellent photosensitization and relatively good stability during the long-term photoreaction process.

ZnPy derivatives of dye-sensitized PCN before and after irradiation for 1 h were desorbed using KOH DMF/water (*v/v* = 1:1) solution (0.1 M) under ultrasonication, and the collected desorbed solutions were determined using UV-vis absorption spectra. As shown in Fig. S12 (ESI[†]), the ZnPy derivatives after the photocatalytic experiments show absorption properties and peak positions that are very similar to those without irradiation, indicating the relatively good stability of the present ZnPy dye-sensitized system. In addition, no absorption signal of the ZnPy derivatives could be detected from the filtrates of the dye-sensitized product suspensions after irradiation, indicating that there is no dye present in the aqueous solution and the dye molecules can be anchored strongly onto *g*-C₃N₄.^{21,22} Moreover, the dye solutions desorbed from the dye-sensitized products before and after irradiation exhibit very similar UV-vis absorption spectra (Fig. S12, ESI[†]), implying that unimpaired skeletons of the ZnPy derivatives during the photoreaction process are present. The above fairly good stability of sensitized PCN could be due to efficient dye regeneration in the presence of AA as a sacrificial reagent.^{20–22}

On the basis of the H₂ evolution activities of the photocatalyst illuminated with various monochromatic light wavelengths (λ = 420, 450, 500, 550, and 600 nm) acquired using their respective narrow band-pass filters, the calculated wavelength-dependent AQY curves are shown in Fig. 8. The AQY values of ZnPy-5/PCN and ZnPy-6/PCN are functions of incident monochromatic light wavelength, and their changing trends are similar to the respective DRS spectra. For instance, ZnPy-5/PCN delivers AQY values of 32.6%, 10.8%, 0.3%, 3.1% and 1.8% when illuminated at 420, 450, 500, 550 and 600 nm monochromatic light, respectively. Similarly, ZnPy-6/PCN delivers AQY values of 33.1%, 11.3%, 0.3%, 3.0% and 2.0% when illuminated at 420, 450, 500, 550 and 600 nm monochromatic

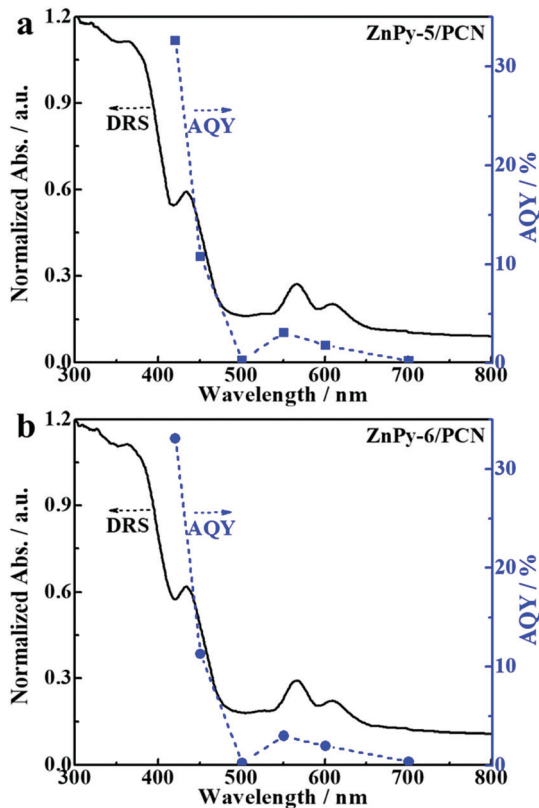


Fig. 8 Comparison of DRS spectra and AQY curves of (a) ZnPy-5/PCN and (b) ZnPy-6/PCN, irradiated by various monochromatic light wavelengths.

light, respectively. It is worth noting that ZnPy-6/PCN exhibits the best AQY value of 33.1% when illuminated at 420 nm monochromatic light, and this is slightly higher than that of ZnPy-5/PCN (32.6%), and much higher than those for ZnPy-1/PCN (10.6%), ZnPy-2/PCN (11.5%) and ZnPy-3/PCN (30.1%), as reported in our previous literature.²⁰

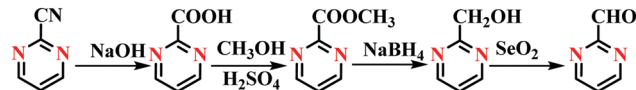
The above results demonstrate that ZnPy-6 is the most efficient sensitizer of $g\text{-C}_3\text{N}_4$ among the synthesized ZnPy derivatives, and that the number and positions of the N atoms in the peripheral substituents of the porphyrin molecules can significantly influence the photoactivity of the corresponding dye-sensitized systems, thus opening up a new path for further improvement of the solar-to-hydrogen energy conversion efficiency of dye-sensitized semiconductors through porphyrin molecular designing.

Experimental section

ZnPy derivative syntheses

2-Pyrimidinecarbaldehyde. This was prepared through a four-step procedure, as shown in Scheme 2.

(1) 2-Cyanopyrimidine (5.0 g, 47.6 mmol) was dropped into NaOH (5.7 g, 142.5 mmol) solution, and then stirred at 65 °C for 4 h. After cooling, the pH value of the mixture was adjusted to ~5.0 using diluted HCl solution, and then the solvent was removed by rotary evaporation. The crude product was washed



Scheme 2 Typical synthetic route for 2-pyrimidinecarbaldehyde.

with methanol several times, filtered and dried by rotary evaporation to obtain the milky-white product (2-pyrimidinecarboxylic acid). Yield: 5.50 g, 90%. ¹H NMR (CDCl₃, 400 MHz): δ = 11.0 ppm (1H), 9.27 ppm (2H), 8.19 ppm (1H).

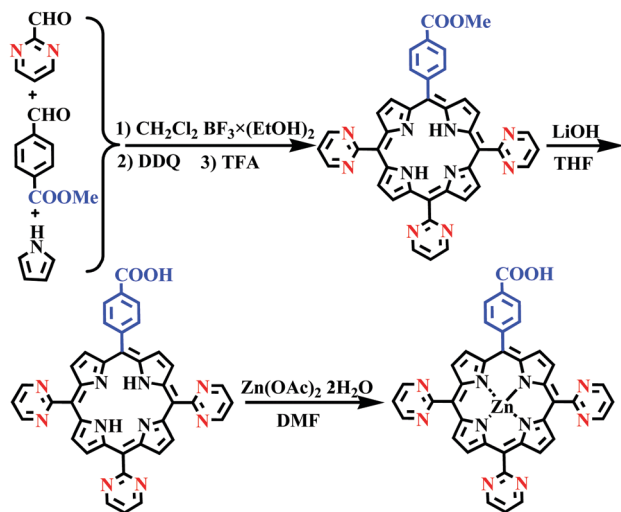
(2) 2-Pyrimidinecarboxylic acid (5.5 g, 44 mmol) was added to 30 mL of methanol and stirred for 10 min, and then 3 mL of concentrated H₂SO₄ solution was dropped into the mixed solution, and this was then refluxed at 85 °C for 2 h. After cooling to room temperature, the solvent was removed by rotary evaporation, and then 20 mL of distilled water was added. After extraction with CHCl₃, the organic phase was dried by rotary evaporation. The crude product was purified by silica gel column chromatography with CH₂Cl₂ and CH₃OH (v/v = 10 : 1) as the eluent to obtain a white solid product (methyl 2-pyrimidinecarboxylate). Yield: 4.40 g, 68%. ¹H NMR (DMSO-d₆, 400 MHz): δ = 9.38 ppm (2H), 7.94 ppm (1H), 4.49 ppm (3H).

(3) Methyl 2-pyrimidinecarboxylate (2.0 g, 14.49 mmol) was added to 32 mL of absolute alcohol under stirring, and then a mixture of NaBH₄ (0.68 g, 20 mmol) and absolute alcohol (32 mL) was dropped into the mixed solution at 0 °C. After reacting for 5 h at room temperature, the solvent was removed by rotary evaporation, and then 6 mL of saturated K₂CO₃ solution was added. After extraction with ethyl acetate, the organic phase was washed and dried with anhydrous Na₂SO₄. The liquid product was collected by rotary evaporation and was then purified by column chromatography to obtain a light-yellow liquid (2-pyrimidinemethanol). Yield: 1.593 g, 84%. ¹H NMR (DMSO-d₆, 400 MHz): δ = 8.79 ppm (2H), 8.79 ppm (2H), 7.41 ppm (1H), 4.95 ppm (2H).

(4) SeO₂ (0.378 g, 3.40 mmol) was added to 15 mL of 1,4-dioxane, and this was then heated at 60 °C for 30 min, before a mixture of 2-pyrimidinemethanol (0.50 g, 4.54 mmol) and 1,4-dioxane (10 mL) was dropped into the mixed solution. During the reaction, the solution changed from cream yellow to reddish brown. After the dropping process, the solution was refluxed at 110 °C for 4 h, and the reaction process was monitored by TLC. After cooling to room temperature, 15 mL of saturated NaCl solution was added. After extraction with CH₃Cl, the organic phase was filtered and collected by rotary evaporation, and it was then dried to obtain a yellowish oily product (2-pyrimidine carbaldehyde). Yield: 0.45 g, 91%. ¹H NMR (DMSO-d₆, 400 MHz): δ = 9.98 ppm (1H), 9.10 ppm (2H), 7.78 ppm (1H).

5-(4-Carboxyphenyl)-10,15,20-tri(2-pyrimidine)porphyrin zinc (ZnPy-5). This was prepared through a three-step procedure, as shown in Scheme 3.

(1) Desiccated CH₂Cl₂ (500 mL) was added into a flask with three necks that was vacuumed and filled with N₂ in advance, and then 2-pyrimidinecarbaldehyde (0.450 g, 4.16 mmol), methyl 4-formylbenzoate (0.341 g, 2.08 mmol) and re-steamed



Scheme 3 Typical synthetic route for ZnPy-5.

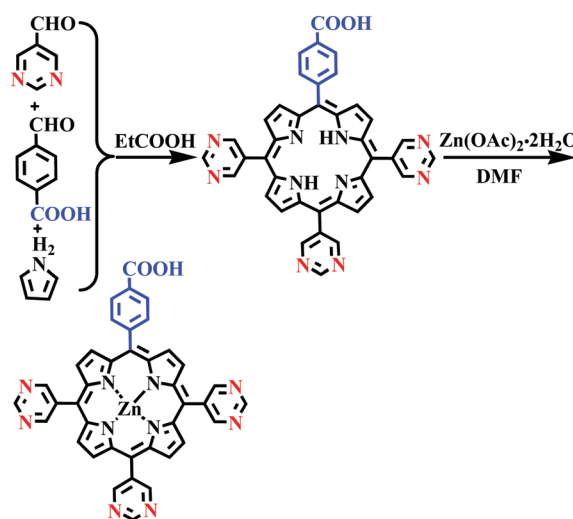
pyrrole (0.388 mL, 5.54 mmol) were added and stirred for 5 min. Afterwards, BF_3 (0.25 g) ether solution was added to the above mixture in the dark, the reaction was kept at room temperature for 1 h, and then 2,3-dicyano-5,6-dichlorobenzoquinone (DDQ, 0.74 g) was added to the reaction solution and stirred at room temperature overnight. After that, 1.0 mL of triethylamine was added to quench the reaction. The resulting crude solid was dried by rotary evaporation and purified by silica gel column chromatography using CH_2Cl_2 and CH_3OH ($v/v = 25:1$) as the eluent to obtain the product [5-(methyl 4-benzoate)-10,15,20-tris(2-pyrimidine)porphyrin]. Yield: 0.15 g, 20.0%. UV-vis λ_{max} (DMF)/nm: 416, 513, 547, 589, 647. ^1H NMR (DMSO- d_6 , 400 MHz): $\delta = 9.41$ ppm (6H, H-Py), 8.94–8.99 ppm (8H, β -H), 8.43 ppm (4H, H-PhCOOMe), 8.03 ppm (3H, H-Py), 4.06 ppm (3H, H-COOMe), -3.00 ppm (2H). TOF-MS (m/z): calc. for $\text{C}_{40}\text{H}_{26}\text{N}_{10}\text{O}_2$ [$M + 1$] $^+$, 679.15; found, 679.02. Elemental analysis calc. for $\text{C}_{40}\text{H}_{26}\text{N}_{10}\text{O}_2 \cdot \text{CH}_3\text{OH} \cdot \text{CH}_2\text{Cl}_2$: C 70.79, H 3.86, N 20.64; found: C 71.03, H 3.90, N 20.34.

(2) 5-(Methyl 4-benzoate)-10,15,20-tris(2-pyrimidine) porphyrin (0.15 g, 0.2 mmol) was dissolved in 15 mL of THF solvent. The resulting solution was dropped into 10 mL of LiOH solution (1.0 M) and then refluxed at 70°C for 10 h. The reaction process was monitored by TLC. Afterwards, the pH of the reaction solution was adjusted to 5.00 using diluted HCl solution, and then extracted three times with ethyl acetate. The collected organic phase was dried with anhydrous Na_2SO_4 and then separated by silica gel column chromatography. The resulting product was re-crystallized using methanol and anhydrous diethyl ether to obtain the final product [5-(4-carboxyphenyl)-10,15,20-tri(2-pyrimidine) porphyrin (H₂Py-5)]. Yield: 60 mg, 47%. UV-vis λ_{max} (DMF)/nm: 416, 511, 546, 587, 642. ^1H NMR (DMSO- d_6 , 400 MHz): $\delta = 9.41$ ppm (6H, H-Py), 8.91–8.96 ppm (8H, β -H), 8.27–8.41 ppm (4H, H-PhCOOH), 8.01 ppm (3H, H-Py), -2.96 ppm (2H). TOF-MS (m/z): calc. for $\text{C}_{39}\text{H}_{24}\text{N}_{10}\text{O}_2$ [$M + 1$] $^+$, 664.21; found, 665.23. Elemental analysis calc. for $\text{C}_{39}\text{H}_{24}\text{N}_{10}\text{O}_2 \cdot \text{CH}_3\text{OH}$: C 68.96, H 4.05, N 20.10; found: C 68.74, H 3.95, N 20.34.

(3) Zinc acetate (0.22 mg, 0.5 mmol) was added to the H₂Py-5 (30 mg, 0.05 mmol) solution of dry DMF (30 mL) under a N_2 atmosphere, and this was then refluxed at 100°C for 10 h. After cooling, the solvent was removed by rotary evaporation. The product was washed with 7 mL water for three times and dried overnight under vacuum to obtain the final product [5-(4-carboxyphenyl)-10,15,20-tri(2-pyrimidine)porphyrin zinc (ZnPy-5)]. Yield: 32 mg, 89%. UV-vis λ_{max} (DMF)/nm: 421, 553, 594. ^1H NMR (DMSO- d_6 , 400 MHz): $\delta = 9.36$ ppm (6H, H-Py), 8.82–8.87 ppm (8H, β -H), 8.21–8.52 ppm (4H, H-PhCOOH), 7.97 ppm (3H, H-Py). TOF-MS (m/z): calc. for $\text{C}_{39}\text{H}_{22}\text{N}_{10}\text{O}_2\text{Zn}$ [$M + 1$] $^+$, 726.12; found, 727.25. Elemental analysis calc. for $\text{C}_{39}\text{H}_{22}\text{N}_{10}\text{O}_2\text{Zn} \cdot \text{CH}_3\text{OH}$: C 58.28, H 3.34, N 16.58; found: C 59.02, H 3.88, N 17.20.

5-(4-Carboxyphenyl)-10,15,20-tri(3-pyrimidine)porphyrin zinc (ZnPy-6). This was prepared through a two-step procedure, as shown in Scheme 4.

(1) 5-Pyrimidinecarbaldehyde (0.648 g, 6.0 mmol) and 4-carboxybenzaldehyde (0.302 g, 2.0 mmol) were added to 80 mL of propanoic acid, and this was then refluxed at 130°C for 1 h. Afterwards, a mixture of re-steamed pyrrole (0.56 mL, 8.0 mmol) and propanoic acid (10 mL) were dropped into the reaction solution, and this was further refluxed at 135°C for 8 h. The solvent was removed by vacuum distillation and the crude product was washed using CH_2Cl_2 to remove the tarry impurity. The collected organic phase was dried by rotary evaporation and purified by silica gel column chromatography using CH_2Cl_2 and CH_3OH ($v/v = 10:1$) as the eluent to obtain a purple product [5-(4-carboxyphenyl)-10,15,20-tri(3-pyrimidine)porphyrin (H₂Py-6)]. Yield: 243 mg, 17%. UV-vis λ_{max} (DMF)/nm: 418, 514, 548, 588, 644. ^1H NMR (DMSO- d_6 , 300 MHz): $\delta = 13.32$ ppm (H, H-COOH), 9.70 ppm (3H, H-Py), 9.67 ppm (6H, H-Py), 8.96–9.04 ppm (8H, β -H), 8.36–8.43 ppm (4H, H-PhCOOH), -2.98 ppm (2H). TOF-MS (m/z): calc. for $\text{C}_{39}\text{H}_{24}\text{N}_{10}\text{O}_2$ [$M + 1$] $^+$, 664.41; found, 665.31. Elemental analysis calc. for $\text{C}_{39}\text{H}_{24}\text{N}_{10}\text{O}_2 \cdot \text{CH}_3\text{OH} \cdot \text{CH}_2\text{Cl}_2$: C 63.00, H 3.87, N 17.92; found: C 63.53, H 4.01, N 18.00.



Scheme 4 Typical synthetic route for ZnPy-6.

(2) Zinc acetate (0.236 g, 1.08 mmol) was added to H₂Py-6 (60 mg, 0.09 mmol) in dry DMF (20 mL) under a N₂ atmosphere, and this was refluxed at 100 °C for 10 h. After being cooled to room temperature and with the addition of 25 mL of distilled water, the resulting purple-green solid was filtered and washed repeatedly with water, and then vacuum-dried to obtain the final product [5-(4-carboxyphenyl)-10,15,20-tri(3-pyrimidine)-porphyrin zinc (ZnPy-6)]. Yield: 42 mg, 64%. UV-vis λ_{max} (DMF)/nm: 427, 558, 599. ¹H NMR (DMSO-d₆, 300 MHz): δ = 9.66 ppm (3H, H-Py), 9.61 ppm (6H, H-Py), 8.87–8.91 ppm (8H, β -H), 8.28–8.42 ppm (4H, H-PhCOOH). TOF-MS (*m/z*): calc. for C₃₉H₂₂N₁₀O₂Zn [M + 1]⁺, 726.13; found, 727.25. Elemental analysis calc. for C₃₉H₂₂N₁₀O₂Zn: C 64.34, H 3.05, N 19.24; found: C 65.02, H 3.35, N 19.58.

Chemical and material characterization

Dichloromethane (DCM), *N,N*-dimethylformamide (DMF) and pyrrole were distilled from CaH₂ under a N₂ atmosphere, and propionic acid was distilled from Na₂SO₄. Column chromatography was performed on a silica gel column (Merck, Kieselgel 60, 70–230 mesh). Thin layer chromatography (TLC) was carried out on a glass plate (20 × 20 cm) using silica gel (GF-254). All reagents and solvents were of pure quality and were used as received, unless otherwise stated.

¹H NMR spectra were recorded using a Bruker Ascend 400 spectrophotometer with DMSO-d₆ as a solvent and tetramethylsilane as the reference. MALDI-TOF-MS was performed using a Bruker BIFLEX III ultrahigh resolution Fourier-transform ion cyclotron resonance (FTICR) mass spectrometer with α -cyano-4-hydroxycinnamic acid as a matrix. UV-vis absorption spectra were recorded using a TU-1810 spectrophotometer. A K2 ISIS spectrometer was used to determine the fluorescence spectra and a Biorad FTS-165 spectrometer was used to record the FTIR spectra using a KBr pellet. A MPC-3100 spectrophotometer was used to record the UV-vis diffuse reflectance spectra (DRS) with BaSO₄ as a reference, and a F-4600 fluorescence spectrophotometer was used to determine the photo-luminescence (PL) spectra. Elemental analyses were carried out using a Vario EL III Elementar. Time-resolved photo-luminescence spectra (TRPS) were recorded on a FL SP920 fluorescence lifetime spectrophotometer (Edinburgh Instruments, UK) at excitation and detection wavelengths of 475 and 610 nm, respectively. The fluorescence lifetime (τ) was calculated according to an exponential fitting equation:⁴⁵

$$\text{Fit} = A + B \times e^{-t/\tau_1} + B_1 \times e^{-t/\tau_2} + B_1 \times e^{-t/\tau_3} \quad (1)$$

where *A*, *B*₁, *B*₂ and *B*₃ are constants and are obtained after fitting the decay curve. The statistic values of the lifetimes were obtained from the fluorescence behavior of 10⁵ photons after excitation by computer software.

Electrochemical measurements

Cyclic voltammetry (CV) measurements were conducted using a CHI600C voltammetric analyzer in a three-electrode setup, which included a glassy carbon electrode, a Ag wire counter electrode and a Ag/Ag⁺ reference electrode (0.01 M AgNO₃ in dry

acetonitrile). The measurements were performed in [NBu₄]-[ClO₄] solution (0.1 M) of dried DMF under a N₂ atmosphere at room temperature with a scan rate of 100 mV s⁻¹. The results were corrected for junction potentials using a normal hydrogen electrode (NHE), which was referenced internally to the ferrocenium/ferrocene (Fc⁺/Fc) couple [*E*_{1/2}(Fc⁺/Fc) = 0.74 V vs. NHE].¹⁵

Materials preparation

g-C₃N₄ was prepared as follows:¹² urea (5.0 g) was placed in a covered crucible and heated at 580 °C for 3 h at a heating rate of 5 °C min⁻¹. After cooling to room temperature, the product was purified using HNO₃ solution (0.1 M) and distilled water, and it was then dried at 70 °C overnight to obtain the yellow-colored g-C₃N₄ (denoted as CN). A Pt co-catalyst was deposited onto g-C₃N₄, as follows:²¹ g-C₃N₄ (0.60 g) was dispersed in a water (150 mL) and methanol (35 mL) mixed solution containing H₂PtCl₆ (0.077 M, 0.60 mL), and then the suspension was irradiated for 3 h using a 500 W Hg-lamp under stirring. The product was collected by centrifugation, washed with water and dried at 70 °C overnight to obtain 1.5 wt% Pt-loaded g-C₃N₄ (denoted as PCN).

Dye-sensitized PCN was prepared as follows:²⁰ the above 1.5 wt% Pt-loaded g-C₃N₄ (PCN, 0.1 g) was added to a ZnPy derivative DMF solution. After stirring for 6 h, rotary evaporation was used to collect the product to ensure the same amount of dye-loading (6.3 $\mu\text{mol g}^{-1}$).

Photocatalytic experiments

The photoreaction for H₂ evolution was performed in a home-made outer-irradiation-type photoreactor (Pyrex glass) connected to a closed gas-circulation system. The amount of H₂ evolution was measured using gas chromatography (GC, SP6890, TCD detector, 5 Å molecular sieve columns and a Ar carrier). In a typical process, the photocatalyst was dispersed in 10 mL of water containing ascorbic acid (AA, 50 mM) as an electron donor, and this was treated in an ultrasonic bath for 20 min before illumination. After thoroughly removing the air, the suspension was irradiated from the top with visible light ($\lambda \geq 420$ nm), which was obtained using a cutoff filter ($\lambda \geq 420$ nm) placed on a 300 W Xe-lamp (PLS-SXE300, Beijing Trusttech Co. Ltd, China).

The apparent quantum yield (AQY) was calculated based on the amount of H₂ evolution per hour obtained under the same photoreaction conditions but with monochromatic light illumination derived from a band pass filter (e.g. $\lambda = 420 \pm 10$ nm) using eqn (2):^{20–23}

$$\begin{aligned} \text{AQY} (\%) &= \frac{2 \times \text{Number of evolved H}_2 \text{ molecules}}{\text{Number of incident photons}} \times 100\% \\ &= \frac{2 \times CN_A}{Pt\lambda/hc} \times 100\% \end{aligned} \quad (2)$$

where *C* is the H₂ production amount per hour ($\mu\text{mol h}^{-1}$); *N*_A is the Avogadro constant ($6.02 \times 10^{23} \text{ mol}^{-1}$); *t* is the light

irradiation time (1 h); λ is the monochromatic light wavelength (nm); h is the Planck constant (6.626×10^{-34} J s); c is the vacuum light velocity (3×10^8 m s⁻¹); P is the irradiation flux (W) on the irradiated area, and is equal to the product of the irradiation area ($A = 11.3$ cm²) and the incident monochromatic light intensity (p , mW cm⁻²) that was detected by a calibrated Si photodiode (SRC-1000-TC-QZ-N, Oriel).

The turnover number (TON) is usually defined by the number of reacted molecules and the number of active sites. In the present work, we assumed that H₂ production takes place when two electrons injected from the excited dye molecules react with two protons. One dye molecule can produce only one photogenerated electron that can be injected into the CB of g-C₃N₄, therefore two dye molecules are needed to react with two H⁺ ions and produce one H₂ molecule, and so the TON can be calculated based the number of evolved H₂ molecules per hour and the active site using eqn (3):²⁷

$$\text{TON} = \frac{2 \times \text{Number of evolved H}_2 \text{ molecules per hour}}{\text{Number of dye molecules adsorbed}} \quad (3)$$

where the evolved H₂ molecules per hour is the H₂ production rate ($\mu\text{mol h}^{-1}$), and the number of dye molecules is calculated from the dye-loading amount ($6.3 \mu\text{mol g}^{-1}$) and the photocatalyst dosage (0.015 g).

Conclusions

Novel asymmetric zinc porphyrin (ZnPy) derivatives (ZnPy-5 and ZnPy-6) bearing one benzoic acid and three pseudo-pyrimidines as *meso*-position substituents were synthesized and utilized to sensitize Pt-loaded g-C₃N₄ (PCN). Among the ZnPy derivatives, benzoic acid acts as an electron-withdrawing/anchoring group and the pseudo-pyrimidines act as electron-donating groups, whereby the photoexcited electrons can be transferred from the metal center of porphyrin towards the carboxyl group and injected into g-C₃N₄ for H₂ evolution. The pseudo-pyrimidines that replace the phenyls (ZnPy-1) or pseudo-pyridines (ZnPy-2 and ZnPy-3) show significantly improved photosensitization on PCN, even though they have very similar photo-absorption abilities and energy band structures. Moreover, the different positions of the two N atoms in the pseudo-pyrimidines resulted in different interactions of the ZnPy derivatives with the sacrificial reagent (AA) and g-C₃N₄, and this then strongly influences the activity. For example, ZnPy-6 with the lowest steric hindrance of N atoms in its pseudo-pyrimidines is easy to combine with g-C₃N₄ and AA, and thus ZnPy-6/PCN exhibits a H₂ evolution production activity of 585 $\mu\text{mol h}^{-1}$ with an extremely high TON of 12 381 h⁻¹, and these values are better than those of ZnPy-5/PCN, which has a H₂ evolution activity of 418 $\mu\text{mol h}^{-1}$ and TON of 8845 h⁻¹. In particular, ZnPy-6/PCN also delivers an impressively high apparent quantum yield of 33.1% at 420 nm monochromatic light, and this is greater than that (32.6%) of ZnPy-5 with a higher steric hindrance. The above differences in photosensitization between ZnPy-5 and ZnPy-6 on PCN can mainly be ascribed to the pseudo-pyrimidines with different N atom positions, leading to

faster electron transfers between ZnPy-6 and g-C₃N₄ than between ZnPy-5 and g-C₃N₄. The present results provide new insight to optimize the porphyrin molecular structure for more efficient combination of the semiconductor and sacrificial reagent, and demonstrate that the N atom number and positions in the peripheral substituents of porphyrins have great influence on photosensitization for H₂ evolution.

Conflicts of interest

There are no conflicts to declare.

Acknowledgements

This work was supported by the National Natural Science Foundation of China (21975190, 21871215, 21573166 and 21271146), the Science & Technology Planning Project of Shenzhen Municipality (JCYJ20180302153921190), the Natural Science Foundation of Jiangsu Province (BK20151247) and the Funds for Creative Research Groups of Hubei Province (2014CFA007), China.

Notes and references

- 1 T. Hisatomi, J. Kubota and K. Domen, *Chem. Soc. Rev.*, 2014, **43**, 7520–7535.
- 2 C. F. Fu, X. J. Wu and J. L. Yang, *Adv. Mater.*, 2018, **30**, 1802106.
- 3 Y. Ma, X. L. Wang, Y. S. Jia, X. B. Chen, H. X. Han and C. Li, *Chem. Rev.*, 2014, **114**, 9987–10043.
- 4 X. B. Chen, S. H. Shen, L. J. Guo and S. S. Mao, *Chem. Rev.*, 2010, **110**, 6503–6570.
- 5 Q. Guo, C. Y. Zhou, Z. B. Ma and X. M. Yang, *Adv. Mater.*, 2019, **50**, 1901997.
- 6 X. H. Zhang, T. Y. Peng and S. S. Song, *J. Mater. Chem. A*, 2016, **4**, 2365–2402.
- 7 Y. Yang, L. C. Yin, Y. Gong, P. Niu, J. Q. Wang, L. Gu, X. Chen, G. Liu, L. Wang and H. M. Cheng, *Adv. Mater.*, 2018, **30**, 1704479.
- 8 Q. Q. Lang, Y. H. Chen, T. L. Huang, L. L. Yang, S. X. Zhong, L. J. Wu, J. R. Chen and S. Bai, *Appl. Catal., B*, 2018, **220**, 182–190.
- 9 S. S. Song, Z. C. Liang, W. L. Fu and T. Y. Peng, *ACS Appl. Mater. Interfaces*, 2017, **9**, 17013–17023.
- 10 S. S. Song, J. M. Wang, T. Y. Peng, W. L. Fu and L. Zan, *Appl. Catal., B*, 2018, **228**, 39–46.
- 11 W. L. Fu, J. M. Wang, S. Y. Zhou, R. J. Li and T. Y. Peng, *ACS Appl. Nano Mater.*, 2018, **1**, 2923–2933.
- 12 Y. Zhang, L. L. Wu, X. Y. Zhao, Y. N. Zhao, H. Q. Tan, X. Zhao, Y. Y. Ma, Z. Zhao, S. Y. Song, Y. H. Wang and Y. G. Li, *Adv. Energy Mater.*, 2018, **8**, 1801139.
- 13 S. X. Min and G. X. Lu, *J. Phys. Chem. C*, 2012, **116**, 19644–19652.
- 14 H. J. Yan and Y. Huang, *Chem. Commun.*, 2011, **47**, 4168–4170.

- 15 L. J. Yu, X. H. Zhang, C. S. Zhuang, L. Lin, R. J. Li and T. Y. Peng, *Phys. Chem. Chem. Phys.*, 2014, **16**, 4106–4114.
- 16 Q. W. Liu, J. M. Wang, D. Liu, R. J. Li and T. Y. Peng, *J. Power Sources*, 2018, **396**, 57–63.
- 17 K. Li, L. Lin, T. Y. Peng, Y. Y. Guo, R. J. Li and J. Zhang, *Chem. Commun.*, 2015, **51**, 12443–12446.
- 18 D. H. Wang, J. N. Pan, H. H. Li, J. J. Liu, Y. B. Wang, L. T. Kang and J. N. Yao, *J. Mater. Chem. A*, 2016, **4**, 290–296.
- 19 O. Bettucci, T. Skaltsas, M. Calamante, A. Dessi, M. Bartolini, A. Sinicropi, J. Filippi, G. Reginato, A. Mordini, P. Fornasiero and L. Zani, *ACS Appl. Energy Mater.*, 2019, **2**, 5600–5612.
- 20 Y. Zheng, J. M. Wang, J. Zhang, T. Y. Peng and R. J. Li, *Dalton Trans.*, 2017, **46**, 8219–8228.
- 21 J. M. Wang, Y. Zheng, T. Y. Peng, J. Zhang and R. J. Li, *ACS Sustainable Chem. Eng.*, 2017, **5**, 7549–7556.
- 22 J. M. Wang, D. Liu, Q. W. Liu, T. Y. Peng, R. J. Li and S. Y. Zhou, *Appl. Surf. Sci.*, 2019, **464**, 255–261.
- 23 Z. F. Wu, X. Li, H. Agren, J. L. Hua and H. Tian, *ACS Appl. Mater. Interfaces*, 2015, **7**, 26355–26359.
- 24 F. Y. Zhang, P. Yu, W. Shen, M. Li and R. X. He, *Comput. Theor. Chem.*, 2016, **1095**, 118–124.
- 25 D. M. Chen, K. W. Wang, W. Z. Hong, R. L. Zong, W. Q. Yao and Y. F. Zhu, *Appl. Catal., B*, 2015, **166–167**, 366–372.
- 26 V. Georgakilas, M. Otyepka, A. B. Bourlinos, V. Chandra, N. Kim, K. C. Kemp, P. Hobza, R. Zboril and K. S. Kim, *Chem. Rev.*, 2012, **112**, 6156–6214.
- 27 Y. Y. Guo, S. S. Song, Y. Zheng, R. J. Li and T. Y. Peng, *Dalton Trans.*, 2016, **45**, 14071–14079.
- 28 K. Pei, Y. Wu, A. Islam, Q. Zhang, L. Han, H. Tian and W. Zhu, *ACS Appl. Mater. Interfaces*, 2013, **5**, 4986–4995.
- 29 B. Liang, C. Y. Jiang, Z. Chen, X. J. Zhang, H. H. Shi and Y. Cao, *J. Mater. Chem.*, 2006, **16**, 1281–1286.
- 30 D. M. de Leeuw, M. M. J. Simenon, A. R. Brown and R. E. F. Einerh, *Synth. Met.*, 1997, **87**, 53–59.
- 31 Y. Ma, P. Zhang, P. H. Zhu, X. Y. Zhang, Y. N. Gao, D. D. Qi, Y. Z. Bian, N. Kobayashi and J. Z. Jiang, *J. Mater. Chem.*, 2011, **21**, 6515–6524.
- 32 J. J. He, G. Benkő, F. Korodi, T. Polívka, R. Lomoth, B. Sun, L. C. Åkermark, A. Hagfeldt and V. Sundström, *J. Am. Chem. Soc.*, 2002, **124**, 4922–4932.
- 33 S. W. Cao, J. X. Low, J. G. Yu and M. Jaroniec, *Adv. Mater.*, 2015, **27**, 2150–2176.
- 34 W. Sinha, M. G. Sommer, N. Deibel, F. Ehret, B. Sarkar and S. Kar, *Chem. – Eur. J.*, 2014, **20**, 15920–15932.
- 35 K. Maeda, M. Eguchi, W. J. Youngblood and T. E. Mallouk, *Chem. Mater.*, 2008, **20**, 6770–6778.
- 36 Y. S. Xu and W. D. Zhang, *ChemCatChem*, 2013, **5**, 2343–2351.
- 37 B. Chai, T. Y. Peng, X. H. Zhang, J. Mao, K. Li and X. G. Zhang, *Dalton Trans.*, 2013, **42**, 3402–3409.
- 38 M. S. Zhu, Z. Li, B. Xiao, Y. T. Lu, Y. K. Du, P. Yang and X. M. Wang, *ACS Appl. Mater. Interfaces*, 2013, **5**, 1732–1740.
- 39 U. Bhattacharjee, L. Men, B. A. Rosales, S. R. Alvarado, J. Vela and J. W. Petrich, *J. Phys. Chem. C*, 2017, **121**, 676–683.
- 40 R. Amorati, A. Baschieri, G. Morroni, R. Gambino and L. Valgimigli, *Chem. – Eur. J.*, 2016, **22**, 7924–7934.
- 41 J. J. Zhu, P. Xiao, H. L. Li and S. A. C. Carabineiro, *ACS Appl. Mater. Interfaces*, 2014, **6**, 16449–16465.
- 42 Q. Li, S. C. Wang, Z. X. Sun, Q. J. Tang, Y. Q. Liu, L. Z. Wang, H. Q. Wang and Z. B. Wu, *Nano Res.*, 2019, **12**, 2749–2759.
- 43 J. W. Fu, J. G. Yu, C. J. Jiang and B. Cheng, *Adv. Energy Mater.*, 2018, **8**, 1701503.
- 44 Y. B. Jiang, Z. Z. Sun, C. Tang, Y. X. Zhou, L. Zeng and L. M. Huang, *Appl. Catal., B*, 2019, **240**, 30–38.
- 45 X. H. Zhang, B. S. Peng, S. Zhang and T. Y. Peng, *ACS Sustainable Chem. Eng.*, 2015, **3**, 1501–1509.